Geometric Frustration of 2D Dopants in Silicon: Surpassing Electrical Saturation

P. H. Citrin,[1] D. A. Muller,[1] H.-J. Gossmann,[1] R. Vanfleet,[2] and P. A. Northrup[1]
[1]*Bell Laboratories, Lucent Technologies, Murray Hill, New Jersey 07974*
[2]*Applied & Engineering Physics, Cornell University, Ithaca, New York 14850*
(Received 28 May 1999)

A novel application of scanning transmission electron microscopy, combined with data from x-ray absorption spectroscopy, establishes that high concentrations of n-type Sb dopants distributed within a two-dimensional (2D) layer in Si can contribute up to an order of magnitude higher free-carrier density than similar dopant concentrations distributed over a three-dimensional region. This difference is explained using a simple model in which formation of electrically deactivating centers is inhibited by solely geometric constraints. It should be possible to extend these ideas for obtaining even higher free-carrier densities in Si from 2D layers of Sb and other group V donors.

PACS numbers: 61.72.Tt, 61.10.Ht, 61.72.Ff, 61.72.Ji

A general problem in semiconductor physics is that free-carrier densities saturate and eventually decrease as dopant donor concentrations increase [1,2]. This behavior in Si has been attributed to the formation of electrically inactive precipitates and/or deactivating dopant centers containing vacancies [2–8]. Recently, a new class of deactivating defects in Si without vacancies, called donor pairs (DP), has been proposed to explain the observed electrical saturation [9]. Formation of DP defects depends only on dopant concentration rather than on sample preparation conditions, so that, even if preparation is adjusted to avoid precipitates or vacancy-containing centers, electrical saturation will still occur. Such a barrier to achieving full electrical activity in highly doped Si should be particularly severe for two-dimensional (2D) δ layers of dopants, where even higher dopant densities can, in principle, be obtained [10]. Free-carrier concentrations, n_e, of up to $\sim 3 \times 10^{14}$ cm^{-2} have been reported in 2D [11], but because the δ-layer thicknesses in those samples were not determined the effective volume concentration of dopants was not known. Conversely, samples from which reliably measured δ-layer widths were reported had no corresponding measurements of electrical activity [12,13]. The importance of DP defects in 2D-doped Si, and thus the inherent limitations on free-carrier densities, in general, has therefore not been possible to assess.

Here, we use a new application of scanning transmission electron microscopy (STEM) for directly measuring the widths of δ layers from samples whose electrical properties have been well determined. This allows a consistent conversion of 2D to 3D dopant concentrations and free-carrier densities. Surprisingly, and contrary to expectations about forming DP defects, we find that electrical saturation in highly 2D-doped Si does *not* occur. Extended x-ray absorption fine structure (EXAFS) measurements confirm that in these samples neither precipitates nor vacancy-containing dopant defects are important. The results are explained using a simple model in which the formation of DP defects in 2D is geometrically frustrated at high dopant concentrations. The model thus predicts that in 2D-doped Si it should be possible to realize almost complete electrical activity even at the highest levels of n-type doping.

To illustrate the basic problem of characterizing dopant activity in 2D, we first show at the top of Fig. 1 an example of electrical saturation for the case of 3D Sb-doped Si. The samples were grown by low-temperature molecular beam epitaxy with the Sb atoms distributed over a 300-Å-wide region [14]. Dopants are confined to a much narrower region in δ-doped samples grown under similar conditions [11]; their dopant and free-carrier concentrations are plotted at the bottom of Fig. 1 in areal rather

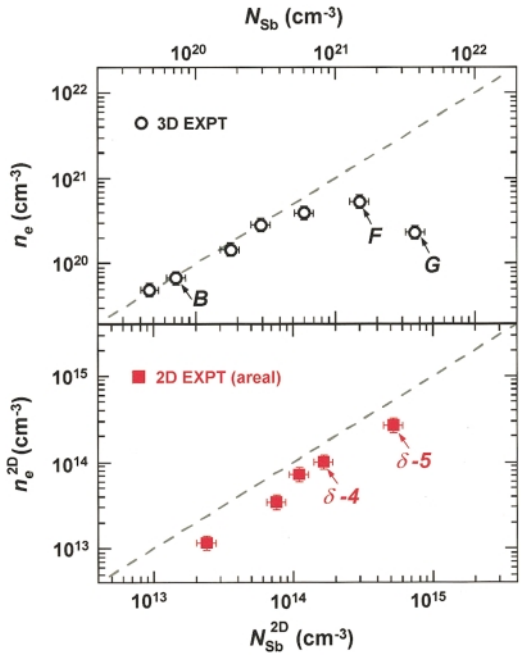

FIG. 1 (color). Free-carrier concentrations, n_e, versus Sb dopant concentrations, N_{Sb}, for Si(100) samples doped in $\sim$300-Å-thick regions (i.e., 3D) and δ layers (i.e., 2D). The sample labels are used for reference, and the dashed lines indicate unity activation.

 0031-9007/99/83(16)/3234(4)$15.00

than volume dimensions. The top and bottom plots span the same change in concentration of 10^3, but the electrical activity in the 3D and 2D samples, n_e/N_{Sb}, exhibits qualitatively very different behavior. Understanding the difference in electrical behavior clearly requires knowing the effective volume concentrations of dopants in the 2D samples, i.e., the widths of the δ layers.

We use a combination of STEM and atomic-scale electron energy loss spectroscopy (EELS) [15–17] to determine the spatial distributions of the δ layers. The Sb atoms are probed at internal interfaces by passing a focused (2–3)- Å-diameter 100-kV electron beam through a film that is thick enough to avoid significant surface state contributions to the transmitted signal, yet thin enough to avoid significant beam spread from multiple scattering. The interface is oriented parallel to the beam to allow atom columns within the interface to be measured separately from atoms in adjacent columns. Viewing the interface in projection means that any interfacial roughness, particularly on length scales thinner than the sample, leads to an apparent broadening of the interface. Accordingly, the δ-layer widths quoted here are upper-limit values.

To map out the spatial distribution of the Sb $M_{4,5}$ EELS edge, which is sensitive only to chemical composition, the δ layer is located using images from the stronger annular dark field (ADF) signal, which is sensitive to both chemical composition [18] and localized strain fields [19,20]. The ADF signal arises from electrons that have undergone Rutherford-like scattering to large angles, resulting in an intensity that is roughly proportional to the square of the atomic number in thin samples. Measurements were performed on the Cornell VG-HB501 STEM equipped with a cold field-emission gun and a McMullan-style parallel EELS spectrometer. Cross-sectioned samples were tripod polished to electron transparency, briefly ion milled, then dipped in HF to remove the damaged surface layer. The EELS spectra were recorded simultaneously with the ADF signal under conditions optimized for atomic resolution imaging. A 100-Å-thick sample is expected to give an ADF resolution of 2.3 Å and an EELS spatial resolution at the Sb $M_{4,5}$ edge of 2.7 Å [21].

The top of Fig. 2 shows the ADF signal for the 2D-doped sample labeled δ-5. Below is the corresponding intensity profile (composition + strain), which closely matches the superposed EELS intensity profile (composition) measured across one of the broadest parts of the δ layer, as shown in the figure. The full width at half maximum (FWHM) of the δ layer seen in the figure varies between 10 and 20 Å, with a mean value of 17 Å over a 50-Å-long region. Examining many such images from different regions in this sample gives an average FWHM value of 16 Å with a standard deviation of 1 Å. Comparable mean values are measured for the other 2D-doped samples.

The measured δ-layer widths allow the 2D dopant and free-carrier areal densities in Fig. 1 to be converted to effective volume concentrations. This is done in Fig. 3,

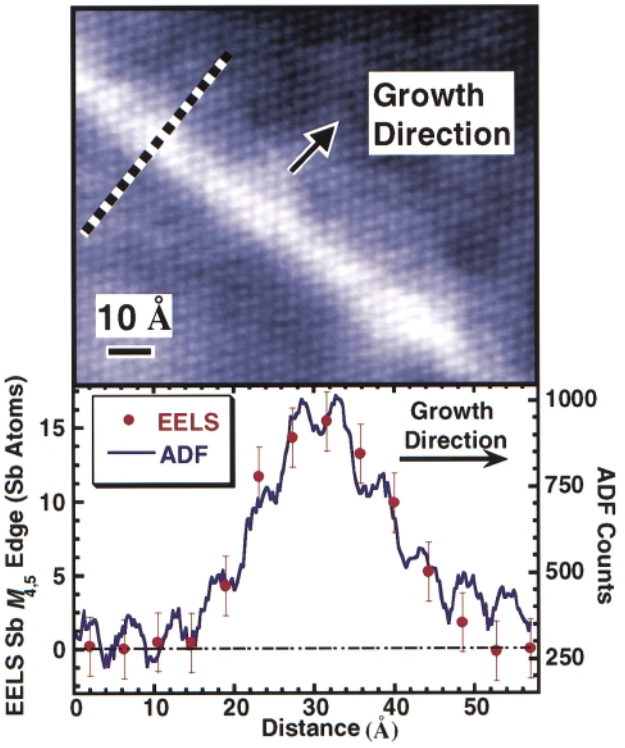

FIG. 2 (color). Measuring the width of a δ layer. Top: annular dark field (ADF) image of the 2D Sb-doped layer in sample δ-5. The Sb atoms appear bright because they scatter more strongly than Si. Bottom: the electron energy loss spectroscopy (EELS) Sb $M_{4,5}$ edge is recorded across the δ layer simultaneously with the ADF signal. The ~500-Å-thick sample, viewed in projection, contains $\lesssim$15 Sb atoms in the beam path.

where the 3D-doped data are included for direct comparison. We see that the highest 2D- and 3D-doped samples, δ-5 and G, respectively, are almost identical in dopant concentrations. On the other hand, the free-carrier concentration in the 2D-doped sample is very different, being almost an order of magnitude higher.

Further confirmation of this striking difference in electrical activity is found in our study of the local structure around Sb from a series of 2D and 3D samples using Sb L_3-edge EXAFS. Fluorescence-detection x-ray absorption measurements from samples cooled $<$50 K (to minimize the effects of thermal disorder [22]) were obtained at the NSLS with the Bell Laboratories X15B beam line [23]. The Fourier transformed (FT) EXAFS data are shown in Fig. 4 for the two highest 2D- and 3D-doped samples. Also included for reference is a low concentration 3D sample, labeled B, containing Sb in only substitutional sites [7,9]. In B, the FT peak at ~2 Å (uncorrected for phase shifts [22]) corresponds exclusively to first-neighbor Si atoms around Sb, while the peak at ~3.4 Å contains unresolved second- and third-neighbor Si atoms. Any surrounding Si atoms not at these distances, or any Sb neighbors within ~4 Å, will lead to destructively interfering EXAFS and a reduction of the FT-peak magnitudes. This

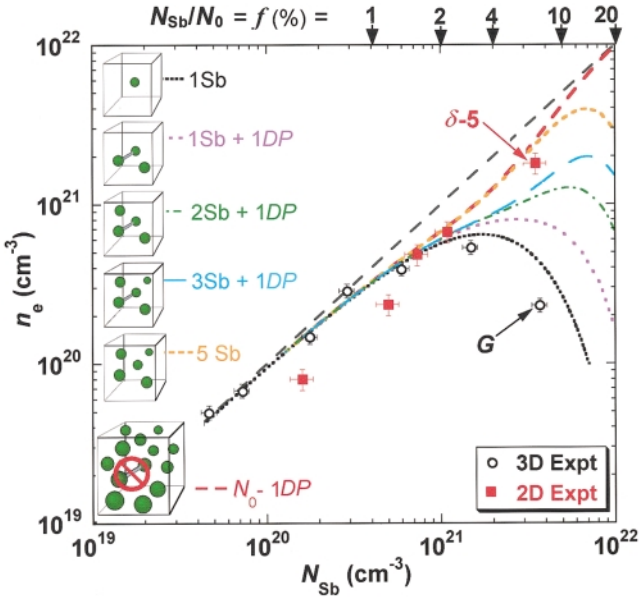

FIG. 3 (color). Direct comparison of experimental free-carrier densities in 2D- versus 3D-doped Si. The differences in electrical behavior agree well with the predictions of a simple model for creating dopant donor-pair (DP) centers, shown schematically here as dumbbells, within Si-lattice cell volumes that are shown schematically here as cubes (see text).

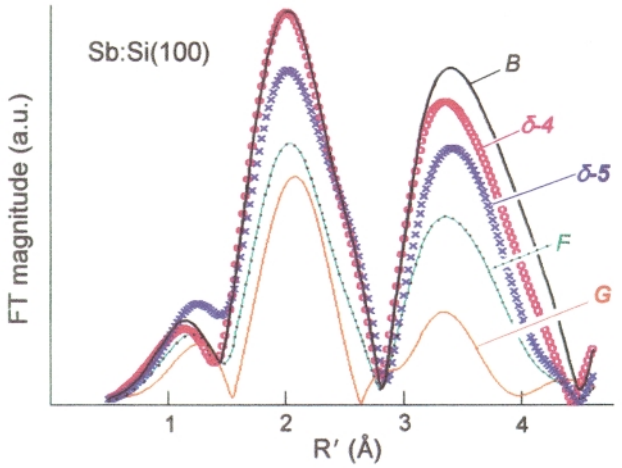

FIG. 4 (color). Fourier transformed Sb L_3-edge EXAFS for different Sb concentrations in the 3D- and 2D-doped Si samples labeled in Fig. 1. The volume concentrations of Sb in δ-5 and G are almost identical.

is observed for both main peaks in the 3D-doped samples [24]. There is also evidence in G of forming a Sb-Sb FT peak at $\sim$2.9 Å [7], signaling the early stages of Sb clustering. By contrast, the 2D-doped samples show much less reduction in the FT peak intensities and no indication of Sb clustering [25]. These results therefore demonstrate that even in highly doped δ layers, the Sb atoms still occupy predominantly substitutional Si sites, consistent with the high electrical activity displayed in Fig. 3.

Why do similarly high concentrations of n-type dopants in Si—differing only in their dimensionality—exhibit such different electrical behavior? Previous work [9] has shown that the dominant mechanism for deactivating free carriers in n-doped Si is the formation of DP defects, provided two conditions are satisfied. First, high annealing temperatures and excess vacancies are avoided in the sample preparation, i.e., formation of inactive precipitates and other deactivating centers is minimal. This is the case for the samples studied here. Second, the doping levels, and thus the number and energy of free carriers at the Fermi level, are high enough to create DP defects. This, too, is the case when $n_e \gtrsim (1\text{–}3) \times 10^{20}$ cm^{-3}, corresponding to the energy range $E_F \approx 0.07\text{–}0.15$ eV needed to create the two lowest-energy DP defects. The formation of these two defects, denoted DP(2) and DP(4) because each contains a pair of substitutional donor atoms separated by second- or "fourth"-neighbor distances [26], involves significant deformation of the surrounding Si lattice. It is therefore appropriate to look for a relationship between the concentration and dimensionality of donor atoms and the ability of the Si lattice to deform and create these defects.

Consider the consequences of randomly distributing N_d dopants in 3D among the N_0 substitutional sites in Si ($N_0 = 5 \times 10^{22}$ cm^{-3}). Any given dopant atom is surrounded by 28 sites, the occupation of which by a second dopant can lead to both dopants becoming electrically inactive, viz., there are 4 first-neighbor sites giving dimers and 24 other sites giving DP(2) and DP(4) defects. The total probability for all configurations in which other dopants occupy any of these 28 special sites can be expressed in terms of the fractional dopant population, $f = N_d/N_0$, by

$$1 = [f + (1 - f)]^{28} = (1 - f)^{28} + 28f(1 - f)^{27} + (28 \cdot 27/2!)f^2(1 - f)^{26} + \ldots . \quad (1)$$

The first term in the expansion represents the probability that no other dopants will occupy any of the 28 special sites around a given dopant, the second that only one other dopant will occupy one of those sites, etc. The contribution to the total free-carrier concentration (absent of any DP defects) is then obtained by multiplying each term by N_d. Previous work on 3D-doped Si considered only the effect of the first term on electrical activity because it dominates when f is small, i.e., $f \lesssim 1/29$, or $\sim$3.5% [9,27]. However, when f is no longer small, not only must the higher-order terms in Eq. (1) be considered but so must the competing interactions between dopants, defects, and the Si lattice.

A simple way to see what happens as f increases is to picture N_d dilute dopants with each one lying at the center of its own 3D Si-lattice volume, or cell, containing the 28 special sites, giving a total of 29 relevant sites per cell per dopant (to simplify our discussion, we ignore dimers). As $f > 1/29$, the probability increases for a second dopant to occupy this cell and form a DP defect, leading always to no free carriers from either dopant. Increasing f still further makes it likely that three dopants can occupy a cell, but now there are (at least) two possibilities to create one

DP defect, leaving one dopant still active. The number of free carriers in this case is represented by multiplying the third term in Eq. (1) by $\frac{1}{3}$. Four dopants per cell leading to one DP defect is represented by multiplying the fourth term by $\frac{1}{2}$, etc. The electrical activities corresponding to configurations with up to 1, 3, 4, or 5 dopants per cell, and at most 1 DP defect, are plotted in Fig. 3. In the left-hand legend, the DP defects are schematically shown as dumbbells, and the cell shapes are schematically shown as cubes with sides $\lesssim 2\sqrt{2}\, a_0$, or $\lesssim 15$ Å, to encompass the DP(4) defects [26]. The increase in electrical activity with dopant density, as each of the higher-order terms in Eq. (1) is included, is apparent.

The calculated activities in Fig. 3 reflect the statistics of occupying particular sites, not of actually forming defects. Increasing the density of dopants also means decreasing the density of ancillary Si atoms needed to create the DP defects through deformation of the surrounding lattice, a factor not included in Eq. (1). Consequently, there must be a threshold in f below which DP defect creation is favored and above which it is inhibited. When f is above threshold in 3D-doped Si, the precipitates offer an alternative to DP defects because their formation requires comparatively less Si deformation; an example of this is seen in sample G. However, above threshold *in 2D-doped Si,* forming DP defects or precipitates is inhibited still further because the choice between which dopants pair up and the ability of the lattice to deform are both constrained by the narrowness of the δ layer, which we directly measure here (in an upper limit) to be comparable to a *single* 3D-cell width, i.e., $\lesssim 15$ Å. In other words, active dopants in 2D, lying anywhere other than at the center of their cells, have fewer options and degrees of freedom than such dopants in 3D, because the number of shared cell faces across which the 2D dopants can form DP defects or precipitates is reduced. Therefore, high concentrations of 2D dopants are more likely to remain electrically active because they are, in effect, *geometrically frustrated*, analogous to antiferromagnetic Ising spins on a triangle [28].

The electrical activity from frustrated dopants has been represented in Fig. 3 by including two additional configurations. One is a cell with up to five dopants and no DP defect, i.e., the sum of the 1st, 3rd, 4th, and 5th terms in Eq. (1) and no corresponding multipliers of $\frac{1}{3}$, $\frac{1}{2}$, and $\frac{3}{5}$, and the other is the asymptotic limit of a cell with up to N_0 dopants and no DP defect, i.e., all terms but the second in Eq. (1). The predicted electrical activity for either configuration is seen to be in very good agreement with that measured for the highest 2D-doped sample studied here. Indeed, the trend towards obtaining even higher free-carrier densities from frustrated dopants is very encouraging.

In conclusion, we have demonstrated a simple and surprising result: Constraining high concentrations of Sb dopants in 2D can strongly inhibit the formation of inactive or deactivating defects in Si, thereby surpassing the barrier to achieving full electrical activity. This finding should also apply to high doping levels of DP-defect-forming P and As dopants, with the understanding that the degree to which electrical deactivation will be inhibited depends on how narrow the δ-layer widths can be prepared.

The authors thank D. J. Chadi and A. Frenkel for helpful discussions. The x-ray absorption measurements were performed at the NSLS, Brookhaven National Laboratory, which is supported by the DOE, Division of Materials Science and Division of Chemical Sciences. R. V. was supported by Air Force Grant No. F49620-95-1-0427. The Cornell STEM was acquired through the NSF (DMR-8314255) and is part of the Cornell CMR (DMR-9632275).

[1] E. F. Schubert, *Doping in III-V Semiconductors* (Cambridge University Press, Cambridge, England, 1993).
[2] R. O. Schwenker, *et al.,* J. Appl. Phys. **42**, 3195 (1971).
[3] A. Nylandsted Larsen *et al.,* J. Appl. Phys. **59**, 1908 (1986).
[4] K. C. Pandey *et al.,* Phys. Rev. Lett. **61**, 1282 (1988).
[5] D. Mathiot and J. C. Pfister, J. Appl. Phys. **66**, 970 (1989).
[6] P. M. Rousseau *et al.,* Appl. Phys. Lett. **65**, 578 (1994).
[7] C. Revenant-Brizard *et al.,* J. Appl. Phys. **79**, 9037 (1996).
[8] M. Ramamoorthy and S. T. Pantelides, Phys. Rev. Lett. **76**, 4753 (1996).
[9] D. J. Chadi *et al.,* Phys. Rev. Lett. **79**, 4834 (1997).
[10] S. J. Bass, J. Cryst. Growth **47**, 613 (1979).
[11] H.-J. Gossmann and F. C. Unterwald, Phys. Rev. B **47**, 12 618 (1993).
[12] W. F. J. Slijkerman *et al.,* J. Appl. Phys. **68**, 5105 (1990).
[13] A. R. Powell *et al.,* J. Cryst. Growth **111**, 907 (1991).
[14] H.-J. Gossmann *et al.,* J. Appl. Phys. **73**, 8237 (1993).
[15] P. E. Batson, Nature (London) **366**, 728 (1993).
[16] N. D. Browning *et al.,* Nature (London) **366**, 143 (1993).
[17] D. A. Muller *et al.,* Nature (London) **366**, 725 (1993).
[18] S. J. Pennycook and D. E. Jesson, Phys. Rev. Lett. **64**, 938 (1990).
[19] D. D. Perovic *et al.,* Ultramicroscopy **52**, 353 (1993).
[20] S. Hillyard and J. Silcox, Ultramicroscopy **58**, 6 (1995).
[21] D. A. Muller and J. Silcox, Ultramicroscopy **59**, 195 (1995).
[22] P. A. Lee *et al.,* Rev. Mod. Phys. **53**, 769 (1981).
[23] A. A. MacDowell *et al.,* Rev. Sci. Instrum. **60**, 1901 (1989).
[24] The reduced FT peak intensities have been shown in Ref. [9] for sample F (where it was labeled H) to be consistent with the formation of DP defects.
[25] EXAFS simulations for different sized Sb clusters, including dimers, were used to rule out the importance of Sb precipitation in the 3D-doped sample F and all of the 2D-doped samples.
[26] The "fourth"-neighbor dopant separation in DP(4) of $\sqrt{2}\, a_0$ (≈ 7.7 Å) is measured in the [110] plane, so it is actually an eighth-neighbor Si distance.
[27] The fractional dopant population must still be large enough to form DP(2) and DP(4) defects, i.e., $f > \sim(3 \times 10^{20})/(5 \times 10^{22}) \approx 0.006$.
[28] A. P. Ramirez, Annu. Rev. Mater. Sci. **24**, 453 (1994).